



HAL
open science

Dispersion of guided-waves in heterogeneous and anisotropic elastic plates: A probabilistic approach

Antoisse Abdoulatuf, Vu-Hieu Nguyen, Christophe Desceliers, Salah Naili

► To cite this version:

Antoisse Abdoulatuf, Vu-Hieu Nguyen, Christophe Desceliers, Salah Naili. Dispersion of guided-waves in heterogeneous and anisotropic elastic plates: A probabilistic approach. *European Journal of Mechanics - A/Solids*, 2022, 91, pp.104382. 10.1016/j.euromechsol.2021.104382 . hal-03519350

HAL Id: hal-03519350

<https://hal.science/hal-03519350>

Submitted on 22 Aug 2023

HAL is a multi-disciplinary open access archive for the deposit and dissemination of scientific research documents, whether they are published or not. The documents may come from teaching and research institutions in France or abroad, or from public or private research centers.

L'archive ouverte pluridisciplinaire **HAL**, est destinée au dépôt et à la diffusion de documents scientifiques de niveau recherche, publiés ou non, émanant des établissements d'enseignement et de recherche français ou étrangers, des laboratoires publics ou privés.



Distributed under a Creative Commons Attribution - NonCommercial 4.0 International License

Dispersion of guided-waves in heterogeneous and anisotropic elastic plates: A probabilistic approach

Antoisse Abdoulouf, Vu-Hieu Nguyen*, Christophe Desceliers and Salah Naili

MSME, CNRS UMR 8208, Univ Paris Est Creteil, Univ Gustave Eiffel, F-94010 Creteil, France

ARTICLE INFO

Keywords:

random plate
functionally-graded
guided waves
dispersion curves
cortical bone
ultrasound

ABSTRACT

In this paper, we present a new approach to study Lamb-type waves of anisotropic elastic plates in a probabilistic framework. The study and analysis are carried out on an elastic plate whose randomly varied elastic properties in the through-thickness direction. By introducing a stochastic model for quantitative description of heterogeneous elastic properties in the plate, the effect of material heterogeneity on Lamb modes may be investigated from a stochastic point of view. To the our best knowledge, this study is the first to investigate Lamb-type waves in a probabilistic framework. Different plate thicknesses are considered and associated dispersion curves are computed. A sensitivity study is performed, highlighting effect of the uncertainty of elasticity properties on the fluctuation of Lamb modes *via* phase velocities, energy velocities and modes shapes. Next, we discuss the relevance of introducing random media to identify branches associated with experimental dispersion curves.

1. Introduction

Ultrasonic Guided-Wave (UGW) method is one of most used methods in the domain of the non-destructive evaluation (NDT) techniques for inspecting and screening the many kinds of natural or artificial structures such as composite beams and shells among which we find, for instance, the railway rails, pipelines transport or long bones in the human body. The method is based on analyzing the mechanical waves that propagate along an elongated structure bounded by its boundaries.


Due to the presence of boundaries (or interfaces), guided-waves are strongly dispersive, *i.e.* their characteristics (phase velocity, energy velocity and attenuation) depend on emitted frequency which may typically vary from hundreds of kilohertz to several megahertz depending on the applications. Mechanical and geometric properties of the medium influence also the dispersion of guided-waves. The study of guided-waves in different media, so-called Lamb wave in isotropic waveguide, was the object of a large number of works in the literature. For a fundamental analysis of guided waves in isotropic/anisotropic plates and cylindrical waveguides, one may refer the reader to the books that serve as benchmarks on the subject [25, 35, 33] for instance. The case partially or totally loaded plates by fluids has been studied by many authors because the energies of waves propagating in waveguides may be radiated into the fluid. This effect is known as leaky Lamb waves for which it has been shown that high density fluids may have a significant influence on the Lamb wave dispersion [24, 9].

As an example of the interest to carry out the study and analyse of Lamb waves in the probabilistic framework, in this paper, we are mainly interested in quantitative ultrasound evaluation of cortical long bones by using the so-called axial transmission techniques [21, 20]. In principle, it is pos-

sible to estimate the material properties of the plate from guided Lamb modes. In this context, many attempts have been done for evaluating bone properties by extracting information from the dispersion of guided waves in long bones [39, 38, 7, 30, 42]. Direct simulations of ultrasound wave propagation in long bones have employed both two-dimensional models [29, 28, 34] or three dimensional ones [2, 8, 22, 32] have been employed. However, most of studies in literature on Lamb waves have been carried out in deterministic frameworks in which material and geometrical properties are given. Nevertheless, for bone tissue, as well as a lot of other materials, experimental observations showed that those properties are not deterministic but random. Thus, it would be necessary to consider the influence of uncertainty of input parameters to the ultrasonic responses. Among the other methods, the probability theory provides an efficient and robust framework to consider the uncertainty of different parameters, which allows us to assess their effects on the quantity of interest. Here, we aim at studying the effect of anisotropy and of heterogeneity of elastic properties in the solid layer on the potentially measured phase velocities. The parametric probabilistic method, which is based on the maximum entropy principle, was used to generate an optimal probabilistic model. This model allows to describe the random tensor field of the elastic moduli in the solid layer by using a minimal set of parameters. Similar models have been developed to investigate the effect of random tensor field of the elastic moduli to the First Arriving Signal (FAS) velocity [13, 14, 23] or to the coefficient of reflection [26]. Note that even though wave propagation problem in random layered media or waveguides has been studied in few works [31, 1, 17, 6, 5, 16, 10], the dispersion of phase and energy velocities in random waveguides, to the best knowledge of the authors, has not been investigated.

This study aims at investigating the sensitivity of dispersion curves of guided-waves in elastic plates according to material heterogeneous random properties. To the our best knowledge, this study is the first to investigate Lamb-type

*Corresponding author

 vu-hieu.nguyen@u-pec.fr (Vu-Hieu Nguyen)

ORCID(s): 0000-0003-1959-9087 (Vu-Hieu Nguyen)

waves in a probabilistic framework. The proposed probabilistic framework, which was presented in our previous work [26] for studying the reflection and transmission coefficients, is employed here to study the phase and group velocities of guided waves in random plates. In this stochastic model, the random tensor of the elastic tensor, of which the mean-value was a transversely isotropic one, becomes anisotropic one and is spatially varied along the thickness direction. The semi-analytical finite element method (SAFE), which has been shown to be very efficient for computing the dispersion curves layered or functionally graded waveguides, was employed.

The paper is organized as follows: In Section 2 the geometry description and governing equations will be presented. Section 3 presents a semi-analytical finite element formulation for determining the dispersion curves. Then, Section 4 presents the procedure used to generate the random elasticity tensor in the thickness direction of the plate. Next, in Section 5, numerical examples on cortical bones are displayed and detailed discussion is provided. Finally, concluding remarks are made in Section 6.

2. Geometry description and governing equation

We consider an infinite solid layer occupying the domain Ω^b with a constant thickness h placed in vacuum, as shown in Fig. 1. The upper and lower plane surfaces of the solid layer Ω^b are denoted by Γ_1^b and Γ_2^b , respectively. Let $\mathcal{R}(O; \mathbf{e}_1, \mathbf{e}_2, \mathbf{e}_3)$ be the Cartesian reference system, where O is the origin of the space and $(\mathbf{e}_1, \mathbf{e}_2, \mathbf{e}_3)$ is the orthonormal basis. The coordinates of a point M are specified by (x_1, x_2, x_3) in \mathcal{R} .

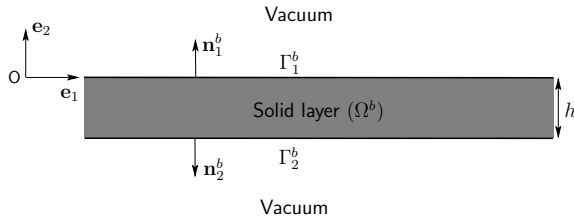


Figure 1: Description of the geometrical configuration.

As a consequence, the displacement component in \mathbf{e}_3 -direction is assumed to be zero and the elastodynamic field will be independent to x_3 due to the source and to the geometrical configuration. Hence, a two-dimensional plane strain problem in the plane $(O, \mathbf{e}_1, \mathbf{e}_2)$ will consider. In what follows, we note respectively ∇ , $\nabla \cdot$ and ∇^2 the gradient, divergence and Laplacian operators in two-dimensional space (2D). The time derivative is denoted by a superimposed dot. We denote respectively by ∂_i and ∂_i^2 the partial derivatives of first and second orders with respect to x_i . In general, the boldface symbols are used to designate the matrices, the fields of vectors and tensors in two-dimensional or three-

dimensional spaces.

In the plane of the plane strains, we denote by $\mathbf{u}(\mathbf{x}, t) = (u_1 \ u_2)^T$ the displacement vector and its components at a point $M \in \Omega_b$ where the superscript “ T ” denotes the transpose operator. By neglecting body forces, the equation of motion in Ω^b is given by:

$$\rho \ddot{\mathbf{u}} - \nabla \cdot \boldsymbol{\sigma} = \mathbf{0}, \quad \forall M \in \Omega^b, \quad (1)$$

where ρ is the volumetric mass density and $\boldsymbol{\sigma}$ is the stress tensor. This equation can be rewritten in a vectorial form:

$$\rho \ddot{\mathbf{u}} - \mathbf{L}^T \mathbf{s} = \mathbf{0}, \quad \forall M \in \Omega^b, \quad (2)$$

where $\mathbf{s} = (\sigma_{11} \ \sigma_{22} \ \sigma_{12})^T$ is the vector of the components of the stress tensor $\boldsymbol{\sigma}$, and the operator \mathbf{L} is defined by:

$$\mathbf{L} = \mathbf{L}_1 \partial_1 + \mathbf{L}_2 \partial_2, \quad \mathbf{L}_1 = \begin{bmatrix} 1 & 0 \\ 0 & 0 \\ 0 & 1 \end{bmatrix}, \quad \mathbf{L}_2 = \begin{bmatrix} 0 & 0 \\ 0 & 1 \\ 1 & 0 \end{bmatrix}. \quad (3)$$

Using the Voigt notation, the constitutive relation of the solid layer is governed by the Hooke’s law which is given by:

$$\mathbf{s} = \mathbf{c} \mathbf{e}, \quad (4)$$

where \mathbf{e} is a vector containing the components of the infinitesimal strain tensor which is defined by

$$\mathbf{e} = (\epsilon_{11} \ \epsilon_{22} \ 2\epsilon_{12})^T = \mathbf{L} \mathbf{u},$$

and \mathbf{c} is the elastic modulus tensor:

$$\mathbf{c} = \begin{bmatrix} c_{11} & c_{12} & c_{16} \\ c_{12} & c_{22} & c_{26} \\ c_{16} & c_{26} & c_{66} \end{bmatrix}. \quad (5)$$

In this study, it is assumed that the elastic constants only depend on x_2 , *i.e.* $\mathbf{c} = \mathbf{c}(x_2)$.

At the surfaces Γ_1^{bv} and Γ_2^{bv} , the free-traction conditions read:

$$\boldsymbol{\sigma} \mathbf{n}_\alpha^b = \mathbf{0}, \quad \forall M \in \Gamma_\alpha^b \quad (\alpha = 1, 2), \quad (6)$$

where \mathbf{n}_α^b is the normal unit vector to the surface Γ_α^b . For the considered plate, $\mathbf{n}_1^b = -\mathbf{n}_2^b = (0 \ 1)^T$, Eq. (6) may be written as follows:

$$\mathbf{t} = \mathbf{0}, \quad \text{at } x_2 = 0 \text{ and } x_2 = -h, \quad (7)$$

where $\mathbf{t} = (\sigma_{12} \ \sigma_{22})^T = \mathbf{L}_2^T \mathbf{s}$. Since $\mathbf{s} = \mathbf{c} \mathbf{e}$ and $\mathbf{e} = \mathbf{L} \mathbf{u}$ into (7), the surface traction vector \mathbf{t} may be expressed in function of \mathbf{u} as follows:

$$\mathbf{t} = (\mathbf{L}_2^T \mathbf{c} \mathbf{L}_1 \partial_1 + \mathbf{L}_2^T \mathbf{c} \mathbf{L}_2 \partial_2) \mathbf{u}. \quad (8)$$

3. Dispersion analysis by using semi-analytical finite element method (SAFE)

3.1. Equations in the frequency-wavenumber domain

We look for the solution of a harmonic wave propagating along the axial direction \mathbf{e}_1 . The wave solution in the solid loyer may be expressed in the following form:

$$\mathbf{u}(M, t) = \hat{\mathbf{u}}(x_2) \exp[i(k_1 x_1 - \omega t)], \quad \forall M \in \Omega^b, \quad (9)$$

where $i^2 = -1$, $\hat{\mathbf{u}} = (\hat{u}_1, \hat{u}_2)^T$, ω is the angular frequency and k_1 denotes the wavenumber in the direction \mathbf{e}_1 . As a result, the time derivative and the spatial differential operator with respect to x_1 turn into simple factors: $\partial_t(\ast) \rightarrow -i\omega(\ast)$, $\partial_1 \rightarrow ik_1(\ast)$. Consequently, the equation of motion (2) can be written as a system of partial differential equations of the displacement $\hat{\mathbf{u}}$ which only respect to x_2 :

$$\begin{aligned} (-\omega^2 \mathbf{A}_1 + k_1^2 \mathbf{A}_2) \hat{\mathbf{u}} - ik_1 \mathbf{A}_3^T \partial_2 \hat{\mathbf{u}} - \partial_2 \hat{\mathbf{t}} &= \mathbf{0}, \\ \forall x_2 \in [-h, 0], \end{aligned} \quad (10)$$

where $\hat{\mathbf{t}} = (ik_1 \mathbf{A}_3 + \mathbf{A}_4 \partial_2) \hat{\mathbf{u}}$ (see Eq. (8)); the two-by-two matrices \mathbf{A}_α ($\alpha = 1, \dots, 4$) are defined by:

$$\begin{aligned} \mathbf{A}_1 &= \rho \mathbf{I}_d, & \mathbf{A}_2 &= \mathbf{L}_1^T \mathbf{c} \mathbf{L}_1, \\ \mathbf{A}_3 &= \mathbf{L}_2^T \mathbf{c} \mathbf{L}_1, & \mathbf{A}_4 &= \mathbf{L}_2^T \mathbf{c} \mathbf{L}_2, \end{aligned} \quad (11)$$

where \mathbf{I}_d is the two-by-two identity matrix.

3.2. Weak formulation and finite element formulation

3.2.1. Weak formulation

The weak formulation of the problem defined from Eq. (10) may be derived using standard procedure used in the finite element method [4]. Let C^{ad} be the admissible function space constituted by all sufficient smooth complex-valued functions $x_2 \in]-h, 0[\rightarrow \delta \mathbf{u}(x_2) \in \mathbb{C} \times \mathbb{C}$, where \mathbb{C} denotes the set of complex numbers. The conjugate transpose of $\delta \mathbf{u}$ is denoted $\delta \mathbf{u}^*$. By multiplying the equation (10) with the test function $\delta \mathbf{u}^* \in C^{ad}$ then integrating by parts, we obtain:

$$\begin{aligned} \int_{-h}^0 \delta \mathbf{u}^* (-\omega^2 \mathbf{A}_1 + k_1^2 \mathbf{A}_2 - ik_1 \mathbf{A}_3^T \partial_2) \hat{\mathbf{u}} dx_2 \\ + \int_{-h}^0 \partial_2 (\delta \mathbf{u}^*) \hat{\mathbf{t}} dx_2 - [\delta \mathbf{u}^* \hat{\mathbf{t}}]_{-h}^0 = 0. \end{aligned} \quad (12)$$

The last term in Eq. (12) may vanish by using the free-surfaces boundary conditions (7). Thus the weak formulation of the problem reads: Find $\mathbf{u} \in C^{ad}$ such that:

$$\begin{aligned} \int_{-h}^0 \delta \mathbf{u}^* (-\omega^2 \mathbf{A}_1 + k_1^2 \mathbf{A}_2 - ik_1 \mathbf{A}_3^T \partial_2) \hat{\mathbf{u}} dx_2 \\ + \int_{-h}^0 \partial_2 (\delta \mathbf{u}^*) (ik_1 \mathbf{A}_3 + \mathbf{A}_4 \partial_2) \hat{\mathbf{u}} dx_2 = 0, \end{aligned} \quad (13)$$

for all $\delta \mathbf{u}^* \in C^{ad}$.

3.2.2. Finite element formulation

The finite element mesh of the linear domain $[-h, 0]$ contains n^{el} elements Ω_e : $[-h, 0] = \bigcup_e \Omega_e$ ($e = 1, \dots, n^{el}$). The Galerkin finite element method is used. Both functions $\hat{\mathbf{u}}$ and $\delta \hat{\mathbf{u}}$ in each element Ω_e are approximated using the same interpolation function:

$$\hat{\mathbf{u}}(x_2) = \mathbf{N}_e \mathbf{U}_e, \quad \delta \mathbf{u}(x_2) = \mathbf{N}_e \delta \mathbf{U}_e, \quad \forall x_2 \in \Omega_e, \quad (14)$$

where \mathbf{N}_e is the interpolation function, \mathbf{U}_e and $\delta \mathbf{U}_e$ are respectively the vectors of nodal solutions of \mathbf{u} and $\delta \mathbf{u}$ in Ω_e . By substituting Eq. (14) into Eq. (13) and assembling the elementary matrices, we obtain the following quadratic eigenvalue problem: Find non trivial triplet $(\omega, k_1, \mathbf{U})$ such that :

$$[-\omega^2 \mathbf{K}_1 + k_1^2 \mathbf{K}_2 + ik_1 \mathbf{K}_3 + \mathbf{K}_4] \mathbf{U} = \mathbf{0}, \quad (15)$$

where \mathbf{U} is the global nodal displacement vector and:

$$\begin{aligned} \mathbf{K}_1 &= \bigcup_e \int_{\Omega_e} \mathbf{N}_e^T \mathbf{A}_1 \mathbf{N}_e dx_2, \\ \mathbf{K}_2 &= \bigcup_e \int_{\Omega_e} \mathbf{N}_e^T \mathbf{A}_2 \mathbf{N}_e dx_2, \\ \mathbf{K}_3 &= \bigcup_e \int_{\Omega_e} 2 \left[\mathbf{N}_e^T \mathbf{A}_3 \mathbf{N}_e \right]_a dx_2, \\ \mathbf{K}_4 &= \bigcup_e \int_{\Omega_e} \mathbf{N}_e^T \mathbf{A}_4 \mathbf{N}_e' dx_2, \end{aligned} \quad (16)$$

in which the notation $[\star]_a$ denotes the antisymmetric part of $[\star]$ and \star' the derivative with respect to x_2 . In this study, Gauss quadrature rule has been used for computing the integrations over the elements.

3.3. Dispersion relation

In order to determine the relation between the angular frequency ω and the axial wavenumber k_1 from the eigenvalue equation (15), two approaches may be used: (i) by fixing the axial wavenumber k_1 , and solving for angular frequency ω (wavenumber sweep), or (ii) by fixing the angular frequency ω , and solving for axial wavenumber k_1 (frequency sweep). In this study, we employed the second one. For a given real value ω , Eq. (15) can be rewritten as the linearized eigenvalue problem which leads to the relation given by:

$$[\mathbf{A}(\omega) - k_1 \mathbf{B}(\omega)] \mathbf{V} = \mathbf{0}, \quad (17)$$

where $\mathbf{A}(\omega)$, $\mathbf{B}(\omega)$ and \mathbf{V} are defined as follows :

$$\mathbf{A}(\omega) = \begin{bmatrix} \mathbf{0} & \mathbf{D} \\ \mathbf{D} & i\mathbf{K}_3 \end{bmatrix}, \quad \mathbf{B}(\omega) = \begin{bmatrix} \mathbf{D} & \mathbf{0} \\ \mathbf{0} & -\mathbf{K}_2 \end{bmatrix}, \quad \mathbf{V} = \begin{bmatrix} \mathbf{U} \\ k_1 \mathbf{U} \end{bmatrix}, \quad (18)$$

with $\mathbf{D} = -\omega^2 \mathbf{K}_1 + \mathbf{K}_4$.

The matrices \mathbf{A} and \mathbf{B} have size of $2N \times 2N$ where N is size of the vector \mathbf{U} , which corresponds to the total number of degrees of freedom of the finite element model. Solution of the characteristic equation $\det[\mathbf{A}(\omega) - k_1 \mathbf{B}(\omega)] = 0$

leads to $2N$ eigenvalues $k_1^{(m)}$ ($m = 1..2N$) and $2N$ associated with modes $\mathbf{V}^{(m)}$. Due to the symmetric of the matrices \mathbf{K}_1 , \mathbf{K}_2 and \mathbf{K}_4 and the anti-symmetric of the matrice (*i.e.* $\mathbf{K}_3 = -\mathbf{K}_3^T$), one can demonstrate that if k_1 is an eigenvalue of (18), $-k_1$ is another eigenvalue as well. Indeed, half of the $2N$ eigenvalues associated with $\text{Re}(k_1) > 0$ physically correspond to the travelling waves in the positive \mathbf{e}_1 -axis while the other half express the backward waves $\text{Re}(k_1) < 0$.

3.3.1. Phase velocity and attenuation

The real and imaginary parts, given respectively by : $(\text{Re}[k_1^{(m)}])$ and $(\text{Im}[k_1^{(m)}])$, of the complex wavenumber $k_1^{(m)}$ represent the wave spatial frequency in \mathbf{e}_1 -direction and the wave amplitude decay of the mode (m), respectively. For a given angular frequency ω , the phase velocity $C_{ph}^{(m)}$ and the attenuation $\text{att}^{(m)}$ of the m -th mode are defined respectively by:

$$C_{ph}^{(m)} = \frac{\omega}{\text{Re}[k_1^{(m)}]} \quad , \quad \text{att}^{(m)} = \text{Im}[k_1^{(m)}] \quad (19)$$

3.3.2. Energy velocity

By definition, the wave energy velocity vector is equal to the Poynting vector (*i.e.* the power flow density vector) divided by the total energy (kinetic and strain) per unit volume. Considering the m -th mode, for which the displacement, the strain and the stress vectors at a point are denoted by $\hat{\mathbf{u}}^{(m)}(x_2)$, $\hat{\mathbf{e}}^{(m)}(x_2)$ and $\hat{\mathbf{s}}^{(m)}(x_2)$, respectively. The temporal average of the kinetic and strain energy densities may be expressed, respectively, as (see *e.g.* [35]):

$$\langle e_k^{(m)} \rangle_T = \frac{1}{4} \rho \omega^2 \text{Re} (\hat{\mathbf{u}}^{(m)} \cdot \hat{\mathbf{u}}^{(m)}), \quad (20)$$

$$\langle e_p^{(m)} \rangle_T = \frac{1}{4} \text{Re} (\hat{\mathbf{s}}^{(m)} \cdot \hat{\mathbf{e}}^{(m)}), \quad (21)$$

where $\langle \star \rangle_T = \frac{1}{T} \int_0^T (\star) dt$ is the temporal average operator over a unit period of time $T = 2\pi/\omega$.

The local complex Poynting vector $\mathbf{P}^{(m)}$ (power flow density vector) of the m -th mode is defined by:

$$\mathbf{P}^{(m)} = -\frac{1}{2} \omega \text{Re} [(\mathbf{L}_1^T \hat{\mathbf{s}}^{(m)}) \cdot \hat{\mathbf{u}}^{(m)}], \quad (22)$$

The energy velocity of m -th mode in \mathbf{e}_1 -direction is then obtained by:

$$V_e^{(m)} = \frac{\int_{-h}^0 [\mathbf{P}^{(m)} \cdot \mathbf{e}_1] dx_2}{\int_{-h}^0 [\langle e_k^{(m)} \rangle_T + \langle e_p^{(m)} \rangle_T] dx_2} \quad (23)$$

The operator and matrices defined in Eq. (3) are used for rewriting Eq. (22)-(20) in matrix forms, next, Gauss quadrature rule has been used for computing the integrations of total energy and Poynting vector over thickness in Eq. (23).

3.4. Mode separation of heterogeneous plates

For a homogeneous plate, in which the plane of material symmetry coincides to the plane of symmetry of the

plate, the mode shapes obtained by solving Eq (17) may be symmetric or antisymmetric depending whether vertical displacement field may be symmetric or antisymmetric with respect to the median plan $x_2 = -h/2$:

- for a symmetric mode (S-mode) : $\hat{u}_1(x_2) = \hat{u}_1(x_2 - h/2)$, $\hat{u}_2(x_2) = -\hat{u}_2(x_2 - h/2)$
- for an anti-symmetric mode (A-mode) : $\hat{u}_1(x_2) = -\hat{u}_1(x_2 - h/2)$, $\hat{u}_2(x_2) = \hat{u}_2(x_2 - h/2)$.

For the stochastic model presented here, the material properties are not homogeneous but heterogeneous. Hence, the perfect symmetric or antisymmetric modes can not generally be achieved. In order to study the influence of heterogeneity on the guided-wave modes, the so-called quasi-symmetric and quasi-antisymmetric modes may be defined basing from following conditions:

- for a quasi-symmetric mode (S-mode) :

$$\int_{-h/2}^0 |u_1(x_2) - u_1(x_2 - h/2)|^2 dx_2 \leq \text{TOL} \times \|U_1\|^2, \\ \int_{-h/2}^0 |u_2(x_2) + u_2(x_2 - h/2)|^2 dx_2 \leq \text{TOL} \times \|U_2\|^2. \quad (24)$$

- for a quasi-antisymmetric mode (A-mode) :

$$\int_{-h/2}^0 |u_1(x_2) + u_1(x_2 - h/2)|^2 dx_2 \leq \text{TOL} \times \|U_1\|^2, \\ \int_{-h/2}^0 |u_2(x_2) - u_2(x_2 - h/2)|^2 dx_2 \leq \text{TOL} \times \|U_2\|^2, \quad (25)$$

where $\|U_1\|^2 = \int_{-h}^0 |u_1(x_2)|^2 dx_2$, $\|U_2\|^2 = \int_{-h}^0 |u_2(x_2)|^2 dx_2$ and TOL is a numerical tolerance value. In this paper, the quasi-symmetric and quasi-antisymmetric modes are also denoted by *S*-modes and *A*-modes, respectively.

4. Stochastic model

4.1. Probabilistic model of the elasticity tensor

This section provides a brief description of the probabilistic model of the random tensor field of the elastic moduli. We only sketch out the main features of the model in the context of this study. This model is proposed by [37] for the construction of the random elastic modulus tensor in order to describe the random heterogeneity in the solid layer along the \mathbf{e}_2 -direction. The maximum entropy principle [18, 19] and the random matrix theory [26] are used in the three-dimensions space to describe the model. Although the random elastic modulus tensor ($n \times n$) has been generated in the three-dimensions space ($n = 6$) with a high value of the spatial correlation lengths in the \mathbf{e}_1 and \mathbf{e}_3 -directions, only heterogeneous six components, which correspond to the ones defined in the plane ($\mathbf{e}_1, \mathbf{e}_2$), are extracted to be used for the

simulations. Indeed, the solid layer is assumed to be invariant in the \mathbf{e}_3 -direction and homogeneous in the \mathbf{e}_1 -direction.

In what follows, the random elastic modulus matrix at x_2 is denoted by $\mathbf{C}(x_2) \in \mathbf{M}_n^+(\mathbb{R})$ and its mean value by $\mathbf{c}(x_2) \in \mathbf{M}_n^+(\mathbb{R})$, where $\mathbb{E}\{\star\}$ designates the mathematical expectation, $\mathbf{M}_n^+(\mathbb{R})$ the set of all the $(n \times n)$ real symmetric positive-definite matrices and \mathbb{R} the set of real numbers. The following relationship must be satisfied by the random elastic modulus matrix $\mathbf{C}(x_2)$: $\mathbb{E}\{\mathbf{C}(x_2)\} = \mathbf{c}(x_2)$. The matrix $\mathbf{c}(x_2)$ can be decomposed into a product of a unique upper triangular real matrix $\mathbf{L}(x_2)$ with strictly positive diagonal entries and its transpose:

$$\mathbf{c}(x_2) = \mathbf{L}^T(x_2) \mathbf{L}(x_2). \quad (26)$$

The random matrix $\mathbf{C}(x_2)$ is parameterized by its mean value $\mathbf{c}(x_2)$, a dispersion level δ , which is a scalar, and a correlation length λ in the \mathbf{e}_2 -direction, which is denoted by $\mathbf{C}(x_2; \mathbf{c}, \delta, \lambda)$ and may be decomposed into the following form:

$$\mathbf{C}(x_2; \mathbf{c}, \delta, \lambda) = \mathbf{L}^T(x_2) \mathbf{G}(x_2; \mathbf{c}, \delta, \lambda) \mathbf{L}(x_2), \quad (27)$$

where $\mathbf{G}(x_2; \mathbf{c}, \delta, \lambda)$, called the stochastic germ matrix, is a homogeneous and normalized non-Gaussian positive-definite matrix-valued second-order random field with values in $\mathbf{M}_n^+(\mathbf{R})$. The dispersion parameter δ controls the dispersion of the random matrix $\mathbf{G}(x_2; \mathbf{c}, \delta, \lambda)$ and must satisfy the following inequality $0 < \delta < \sqrt{(n+1)/(n+5)}$, which allows the mean-square convergence condition for the germ matrix to be hold [36]. It is proved that the dispersion parameter δ is related to a parameter δ_C , which evaluates the dispersion of the random matrix $\mathbf{C}(x_2)$ by the relation given by:

$$\delta_C(x_2) = \frac{\delta}{\sqrt{n+1}} \left\{ 1 + \frac{\{\text{Tra}(\mathbf{c}(x_2))\}^2}{\text{Tra}([\mathbf{c}(x_2)]^2)} \right\}^{1/2}, \quad (28)$$

The correlation length λ , which is a scalar, is a measure of the distance up to which one has spatial memory of the spatial variations in the material properties.

4.2. Stochastic solver and convergence analysis

The Monte Carlo numerical method is used as the stochastic solver of the problem. For a given parameter set \mathbf{c} , h , δ and λ , the one-dimensional domain $[-h, 0]$ is discretized by using quadratic Lagrangian elements. The global x_2 -coordinates of the Gauss points in all elements are denoted by x_2^β for $\beta = 1, \dots, n_{gp}$, where n_{gp} is the total number of the Gauss points in the mesh.

Let n_r be the total number of realizations, we may construct the set of the independent realizations $\mathbf{C}^{[j]}$ ($j = 1..n_r$) as follows:

$$\mathcal{A} = \left\{ \left\{ \mathbf{C}^{[1]}(x_2^\beta) \right\}_{\beta=1, \dots, n_{gp}}, \dots, \left\{ \mathbf{C}^{[n_r]}(x_2^\beta) \right\}_{\beta=1, \dots, n_{gp}} \right\} \quad (29)$$

in which $\mathbf{C}^{[j]}(x_2^\beta)$ ($\beta = 1, \dots, n_{gp}$) is j -th statistically independent realization of random elastic modulus tensor field \mathbf{C}

indexed by $[-h, 0]$ at points x_2^β as described in Section 4.1 (see [37] and [14]). For each statistical independent realization, the random phase velocity $C_{ph}^{[j]}$, the random energy velocity $V_e^{[j]}$ and the associated mode shape $\mathbf{U}^{[j]}$ may be calculated by using the semi-analytical finite element (SAFE) procedure presented in the previous section.

Convergence analysis with respect to the number of realizations n_r may be performed by studying the convergence of statistical estimates of the second-order moments of random fields (phase velocity, energy velocity and displacement). For instance, the second-order moment of random phase velocity of a given Lamb mode at a fixed frequency is defined by:

$$\text{Conv}_{C_{ph}}(n_r) = \left\{ \frac{1}{n_r} \sum_{j=1}^{n_r} [C_{ph}^{[j]}]^2 \right\}^{1/2}. \quad (30)$$

5. Numerical results

Although the framework presented in this paper aims at the study of a wide variety of wave-guides with random functionally graded properties, the numerical examples presented in this section will focus on studying cortical bone long bones in the context of quantitative ultrasound characterization by using the axial transmission technique. Bone tissue has been shown to be a heterogeneous, anisotropic and porous material. Osteoporosis in long bone may reduce bone's layer thickness and bone's rigidity by increasing porosity, especially in the endosteal region, and by degrading the mineral content of bone matrix. In the context of bone characterization using axial transmission technique, ultrasound responses of cortical bones plates have been investigated in the time domain [12, 28, 29, 34] and frequency domains [3]. In most studies, the bone plate has been considered as a medium whose the material properties are determinist and perfectly known. Recently, probabilistic studies have been conducted by our group to examine the effect of the random heterogeneity in bone plates to different ultrasound responses such as the FAS velocity or the reflection coefficient. The dispersion of guided-waves, which has been shown to be able to provide richer information on the characteristics of bone plates [32, 40, 21], has still not been investigated from a probabilistic point of view.

5.1. Deterministic homogeneous model

Before investigating the ultrasonic behavior of plates whose the material properties are uncertain, we begin with presenting some typical results of homogeneous models. Basically, cortical bone material may be assumed to have a transversally isotropic (TI) elastic properties. In this study, the mean model of the bone plate is considered as a TI elastic homogeneous plate of which the isotropy plane is the cross-section one ($\mathbf{e}_2 - \mathbf{e}_3$). We use typical values for cortical bones, which are taken from the mechanical test results obtained by [15], as follows: $\rho = 1722 \text{ kg.m}^{-3}$, $c_{11} = 23.05 \text{ GPa}$, $c_{22} = 15.1 \text{ GPa}$, $c_{12} = 8.71 \text{ GPa}$, $c_{66} = 4.7 \text{ GPa}$ Note

that the other components of the elastic modulus tensor are given by $c_{22} = c_{33}, c_{12} = c_{13} = c_{21} = c_{31}, c_{23} = c_{32}$ and $c_{55} = c_{66}$. Figures 2(a,b) show the typical relationship between the phase velocities and energy velocities and frequency obtained by using SAFE method. Three homogeneous plates corresponding to different values of the thickness (1 mm, 2 mm, and 4 mm) have been considered. One can observe that thinner plates have less propagation modes than the thicker ones. A convergence study has been performed on the accuracy of SAFE solutions and the analytical one obtained by using the software DISPERSE (data not shown). For the 4mm-thickness plate, the SAFE method needs 24 quadratic elements to capture all modes in frequency range of 0-2 MHz. It is worth noting that, as the considered transversely isotropic plate is homogeneous, the graphs of the phase velocity C_{ph} corresponding to these 3 thickness cases do coincide if C_{ph} is plotted with respect to $f \times h$ instead of f [33].

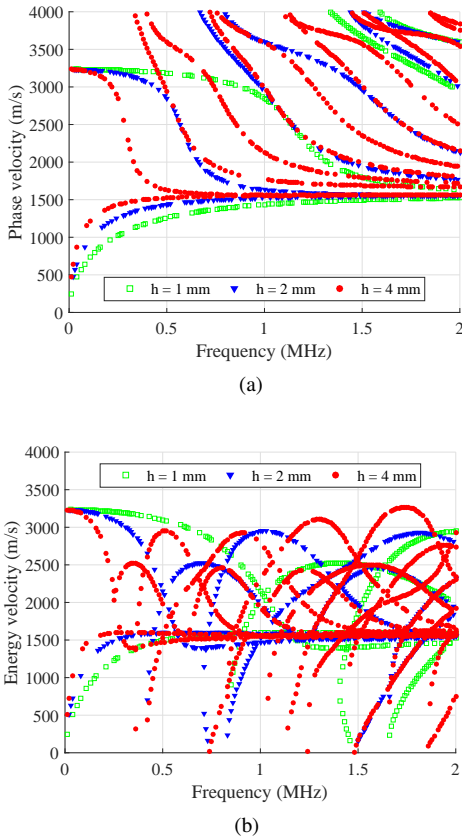


Figure 2: (a) Phase velocity dispersion curves in deterministic models. (b) Energy velocity dispersion curves in deterministic models.

Each point on the dispersion curves of phase velocity (or of energy velocity) corresponds to a particular vibration mode. Figure 3 depicts the solutions of normalized displacements associated with A_0, S_0, A_1, S_1, A_2 and S_2 modes, respectively. The symmetric (S-modes) and anti-symmetric (A-modes) features of these modes may be clearly identified

from these graphs.

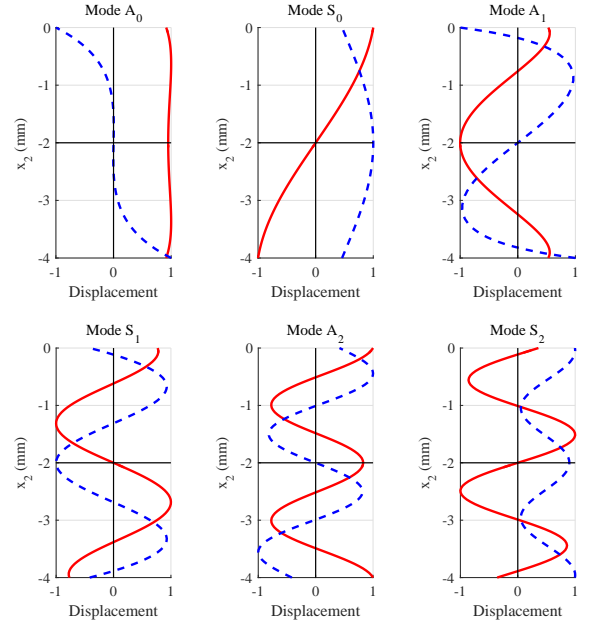


Figure 3: (Color online) Displacement profiles of A_0, S_0, A_1, S_1, A_2 and S_2 modes, taken on the dispersion curves of 4mm-thickness homogeneous bone plate. Dotted blue lines present the component u_1 and the solid red lines show the u_2 one.

5.2. Stochastic heterogeneous model

For the stochastic model, one dispersion value δ and one correlation length λ are used to control the statistical fluctuations of the elastic modulus tensor in the \mathbf{e}_2 -direction. A fixed correlation length $\lambda = 100 \mu\text{m}$ is used, which may be seen as a center-to-center distance between osteons in cortical bone (see [11], [41] and [27]). The dispersion level will be varied from $\delta = 0.1$ to $\delta = 0.3$ to investigate the effect of elasticity's random fluctuation on the quantities of interest which are the phase and energy velocities. For each realization, the procedure presented in Section 3.4 was applied to distinguish the different modes.

5.2.1. Stochastic convergence analysis

In order to study the statistical estimators of the interest quantities, a stochastic convergence analysis must first be carried out. Convergence with respect to number of realizations n_r is performed in studying the convergence of the estimated second-order moment. Stochastic convergence analysis leads to determine the minimal number of realizations to accomplish by using the Monte Carlo solver.

For instance, let us consider a 1mm-thickness solid layer with a dispersion parameter $\delta = 0.3$. This layer is discretized into 50 quadratic elements, which impose at least 5 elements per correlation length ($\lambda = 0.1 \text{ mm}$). Figure 4 shows the graphs of function $n_r \rightarrow \text{Conv}_{C_{ph}}(n_r)$ for symmetric zero-order mode A_0 (see Fig. 4(a)) and antisymmetric zero-order

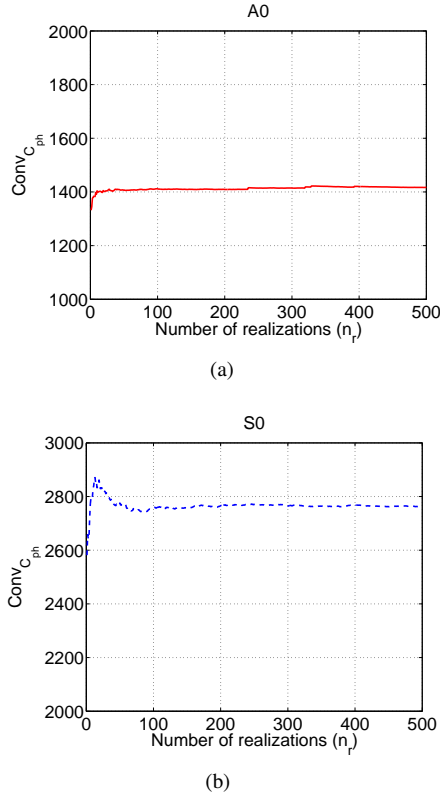


Figure 4: (a): antisymmetric zero-order mode A_0 . (b): symmetric zero-order mode S_0 . $f = 1$ MHz and $\delta = 0.1$.

mode S_0 (see Fig. 4(b)) at a fixed frequency. It can be observed that the graph of $n_r \mapsto Conv_{C_{ph}}(n_r)$ converges with n_r . The fluctuation of statistical estimator of the variance of phase velocity of S_0 -mode is more important than the one of A_0 -mode. Convergence is reached when $n_r \geq 200$ and $n_r \geq 300$ for A_0 and S_0 modes, respectively. Basing on these convergence studies, one may expect that the phase velocity of S_0 mode is more dispersive than A_0 mode from statistical point of view.

5.2.2. Dispersion of phase velocity

In this section, we examine the phase velocity of guided waves in the random plate with different thicknesses h ($h = 1$ mm, $h = 2$ mm and $h = 4$ mm) for which the deterministic results have been shown in Fig. 2. For each thickness case, we consider by 3 random dispersion levels: $\delta = 0.1$, $\delta = 0.2$ and $\delta = 0.3$. Figures 5-7 depict the phase velocity computed by all Monte-Carlo realizations for all combination of h and δ . Note that only propagating modes, which have zero or very small attenuation are displayed. By paying attention to the first fundamental modes, a zoom is shown from Figs. 5-7 to display in more detail the branches of A_0 and S_0 modes.

For a 4mm-thickness plate, the results depicted in Figs. 5 show that the fluctuation of the phase velocity is strongly affected by the heterogeneity along the thickness direction. For all propagating modes, higher dispersion level δ causes higher fluctuations in estimated phase velocity. Meanwhile,

the pattern of dispersion curves is globally unchanged. For a small value of the dispersion level ($\delta = 0.1$), random fluctuations of the phase velocity are small then the modes may still be distinguished. When δ becomes greater ($\delta = 0.2$ and $\delta = 0.3$), random fluctuations of the phase velocity become more and more important and it is harder to distinguish different branches, especially at high frequency region. As it can be expected, guided-wave phase velocity is more sensitive to the heterogeneity in the plate at higher frequency. Certain propagating modes, for which the wavenumbers are real in the mean (homogeneous) model, may be attenuated as the wavenumbers become complex in the heterogeneous model.

Moreover, the modes of higher order may be observed to be more sensitive to the parameter δ . This may be explained by fact that, higher order modes have shorter wavelengths in the e_2 -direction (see Fig. 9). For a given dispersion parameter δ , one can observe in the zoomed part in Fig. 5 that the S_0 -mode is more dispersive than A_0 -mode in the considered frequency range. This effect can be checked from probability density functions (PDF) presented in Fig. 8. At a given frequency, the support of S_0 -mode's PDFs are much larger than the one of A_0 -mode.

Similar remarks regarding to the fluctuation of phase velocity may be made by considering the 2mm- and 4mm-thickness plates. By comparing these 3 cases, we can see that for a same mode at a same frequency, fluctuations of thinner plates are more important than the one of thicker plates. In the case of 1mm- and 2mm-thickness plates, some modes, whose the patterns are completely separated from in each to other in the case of homogeneous plates (e.g. modes A_1 and S_1), may have overlap regions.

In a homogeneous plate, the phase velocity C_{ph} of Lamb waves is a constant whose the value is calculated from the relation $h \times f$. For a heterogeneous plate, the fluctuation of C_{ph} can be observed to be depending of the thickness. For a given mode, the fluctuation of C_{ph} of a thin heterogeneous plate generally is less significant than the one of a thicker plate. In fact, the random variation of mechanical properties in a thick plate has less effects on guided-wave modes reflecting in this way the global dynamic behavior of the plate. By considering a fluctuation level $\delta = 0.1$, Figs. 8(a), (b) and (c) respectively present the probability density functions (PDF) of phase velocities of modes A_0 and S_0 of the 3 thicknesses ($h = 4$ mm, 2 mm, and 1 mm) at 3 different frequencies ($f = 0.25$ MHz, 0.5 MHz and 1 MHz, respectively) so that $h \times f$ has a same value: $h \times f = 1$ (mm \times MHz). As mentioned before, while the dispersion curve of the homogeneous plate is unchanged by fixing $h \times f$, the PDFs of the phase velocity of heterogeneous plates are not the same for the different thicknesses.

5.2.3. Mode shapes

The effect of random variation of mechanical properties on the mode shapes has also been studied. First, we picked one of the realizations calculated for a 4mm-thickness heterogeneous plate with $\delta = 0.3$ and visualized the com-

Dispersion of guided-waves in random plates

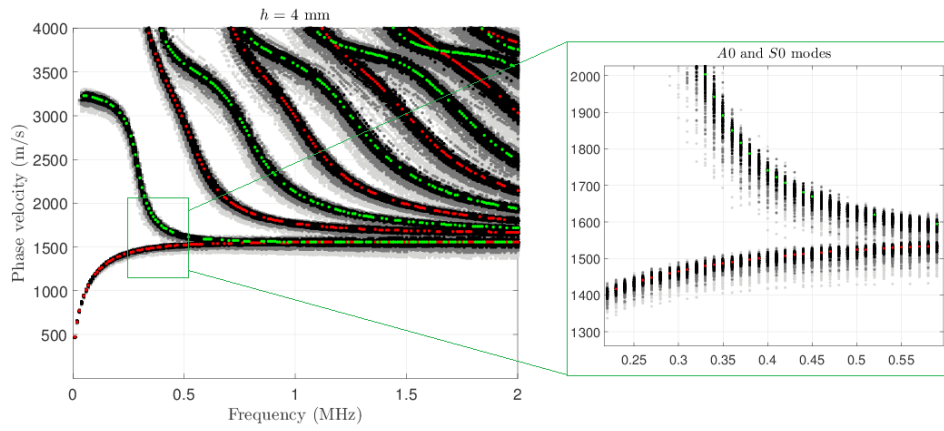


Figure 5: (Color online) Phase velocity of a 4mm-thickness plate with 3 dispersion levels: $\delta = 0.1$ (black region), $\delta = 0.2$ (dark gray region) and $\delta = 0.3$ (light gray region).

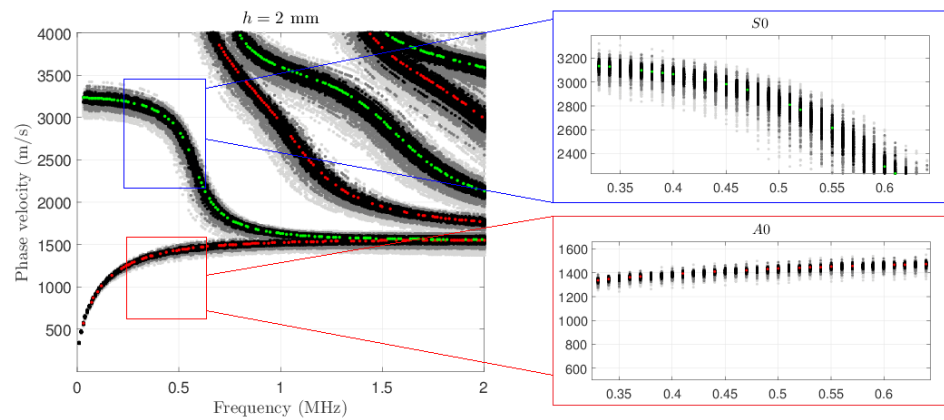


Figure 6: (Color online) Phase velocity of a 2mm-thickness plate with 3 dispersion levels: $\delta = 0.1$ (black region), $\delta = 0.2$ (dark gray region) and $\delta = 0.3$ (light gray region).

ponents (u_1 and u_2) of the normalized displacement eigenvector (see Fig. 9). Due to the heterogeneity, the modes lost their perfect symmetric or anti-symmetric features as shown in case of a homogeneous plate (see Fig. 4). How-

ever, by studying the variation of $u_1(x_2)$ and $u_2(x_2)$, we could identify them by using the quasi-symmetric (S) or quasi-antisymmetric (A) modes, respectively.

In Figs. 10 and 11, the confidence regions of the first six

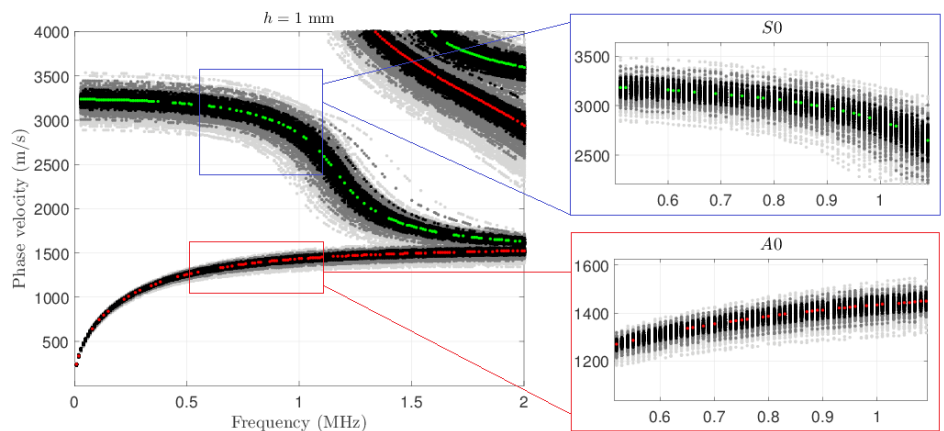


Figure 7: (Color online) Phase velocity of a 1mm-thickness plate with 3 dispersion levels: $\delta = 0.1$ (black region), $\delta = 0.2$ (dark gray region) and $\delta = 0.3$ (light gray region).

Dispersion of guided-waves in random plates

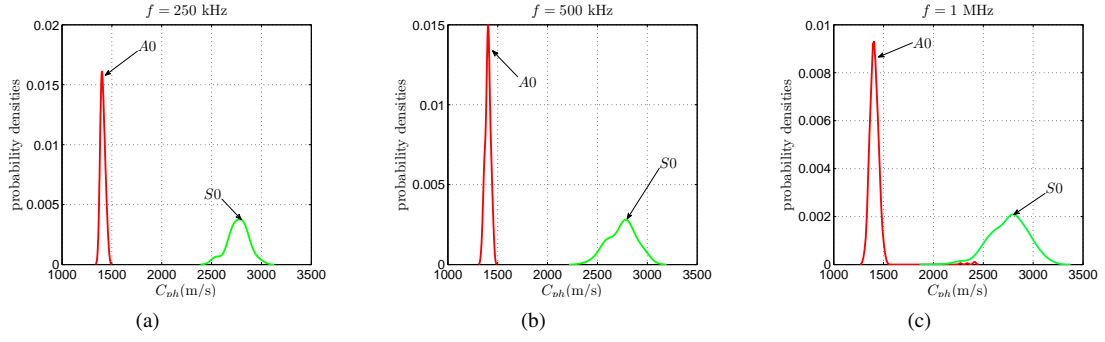


Figure 8: (Color online) Probability density functions of A_0 and S_0 modes for (a) $h = 4$ mm, $f = 0.25$ MHz; (b) $h = 2$ mm, $f = 0.5$ MHz; and (c) $h = 1$ mm, $f = 1$ MHz.

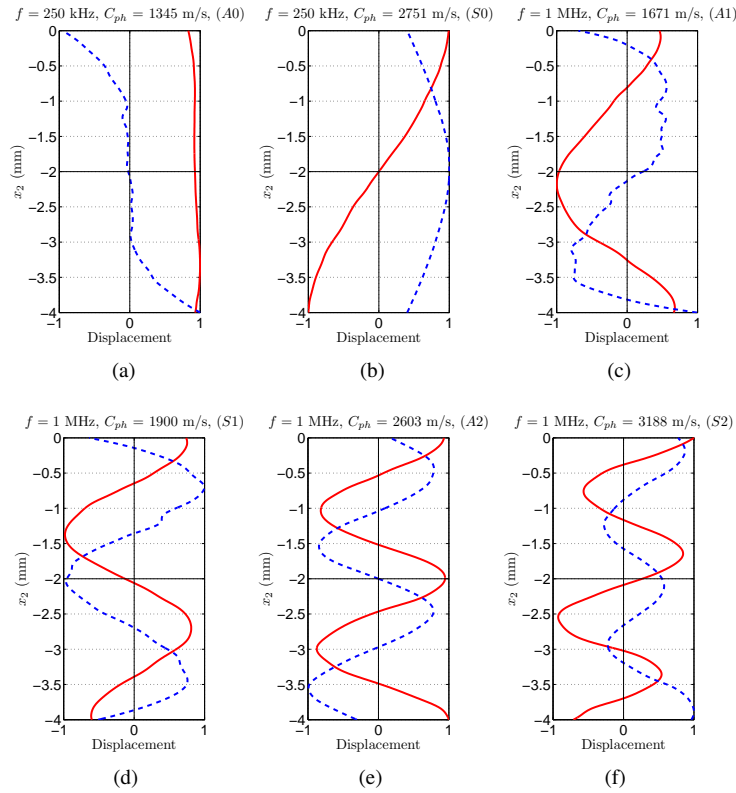


Figure 9: (Color online) Displacement modes at six points taken on the dispersion curves of 4mm-thickness random plate ($\delta = 0.3$); Dotted blue lines represent the component u_1 and the solid red lines show the u_2 one. From (a) to (f) are plotted A_0 , S_0 , A_1 , S_1 , A_2 and S_2 modes, respectively.

mode shapes are shown. Confidence regions associated with a probability level $P_c = 0.95$ for random fields u_1 and u_2 are calculated by using the quantile method (see Appendix A). These results allow us to confirm the nature of captured modes. As observed for the phase velocity, from a probabilistic point of view, the mode shape of S -modes is more dispersive than the ones of A -modes.

5.2.4. Energy velocity

In order to illustrate the behavior of the energy velocity travelling across the cross-section of the plate, the energy velocity V_e on the random plate is presented. For each realization of the random elastic modulus tensor, by using Eq. (23), we can extract energy velocity dispersion curves. For illustration purpose, the graphs of the energy velocities for a heterogeneous plate are presented in Fig. 12. The velocities obtained with the deterministic model are plotted using a cyan color marker. For each frequency, Fig. 13 allows to

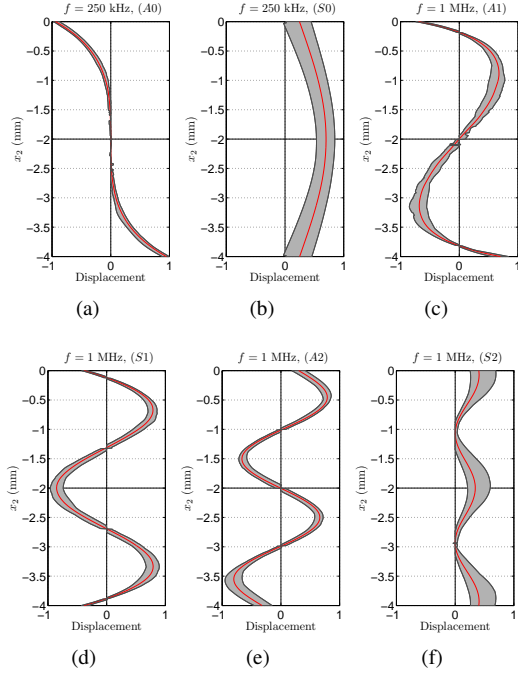


Figure 10: Confidence regions of u_1 ; modes A_0 , S_0 , A_1 , S_1 , A_2 and S_2 modes are plotted from (a) to (f), respectively; the red solid line represents the mean estimated solutions.

know the velocities at which Lamb waves travel along the plate waveguide.

In order to explore the energy contribution when random properties are assumed, we plot energy velocities of all Lamb modes detected at a fixed frequency window. Thus, velocities $V_e^{(m)}$ for the m -th guided-waves are plotted when $\delta = 0.1$ (black region), $\delta = 0.2$ (dark gray region) and $\delta = 0.3$ (light gray region). In the Figs. 12 and 13, it can be seen that, as for the phase velocity dispersion curves, the energy velocity dispersion curves have about complete branches when heterogeneous properties are assumed. Moreover, by increasing the dispersion parameter, the complementary dispersion (*i.e.* the dispersion due to the random fields) increases. Nevertheless, the obtained curves remain coherent with the results obtained with the deterministic model. That is to say, prediction on unknown velocities can also be performed. Hence, the proposed method could allow to predict with sufficiently accuracy, *i.e.* without overestimating or underestimating, the rate at which the energy contribution is propagating in the plate waveguide.

6. Conclusion

In order to interpret the guided-wave data probed using non-destructive techniques, an understanding of dispersion mechanism of wave propagation is necessary. This step remains a challenging area of research due to the complexity of the structures such as the irregularity of geometry, anisotropy, heterogeneity, viscosity, etc. In this paper, we

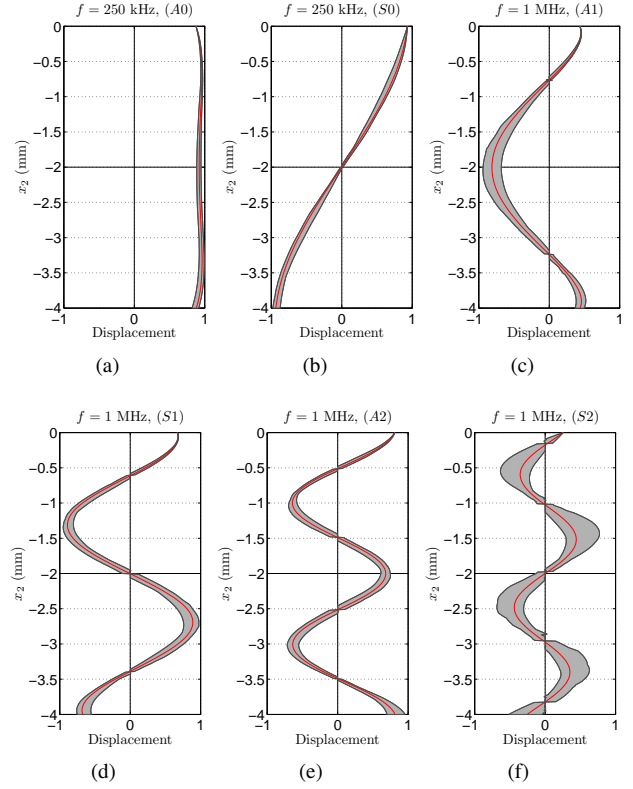


Figure 11: Confidence regions of u_2 ; modes A_0 , S_0 , A_1 , S_1 , A_2 and S_2 are plotted from (a) to (f), respectively; the red solid line represents the mean solutions.

proposed a probabilistic framework to study the effect of the in-depth heterogeneity of elastic properties in an anisotropic elastic plate to the guided wave dispersion characteristics. As the components of the elastic modulus tensor are randomly fluctuated along the thickness's direction, the dispersion equation was not solved by using analytical methods but by the so-called semi-analytical finite element (SAFE) method. It has been shown that the SAFE method is appropriate to derive the dispersion curves as well as the mode shapes of guided-waves in strongly heterogeneous plates.

The Monte Carlo statistical analysis of two fundamental dispersive modes A_0 and S_0 showed that the fluctuation of S_0 mode due the random heterogeneity is much larger than the A_0 's one. The higher order modes A_1 , S_1 , A_2 and S_2 are even more influenced by the random fluctuation of elastic properties in the structure, showing that it would be difficult to identify certain higher modes, especially at the high frequency range. Moreover, it has been shown that A_0 and S_0 modes are more sensitive when the thickness changes.

This study has a few limitations. First, a free bone plate, which may only represent *in vitro*, has been studied. For the *in vivo* tests, the effect of soft tissue and marrow should be considered, even though it has been reported in the literature that soft tissue does not have significant effect on the estimation of mechanical properties of the cortical long bone tissues. Second, in this preliminary study, we only consid-

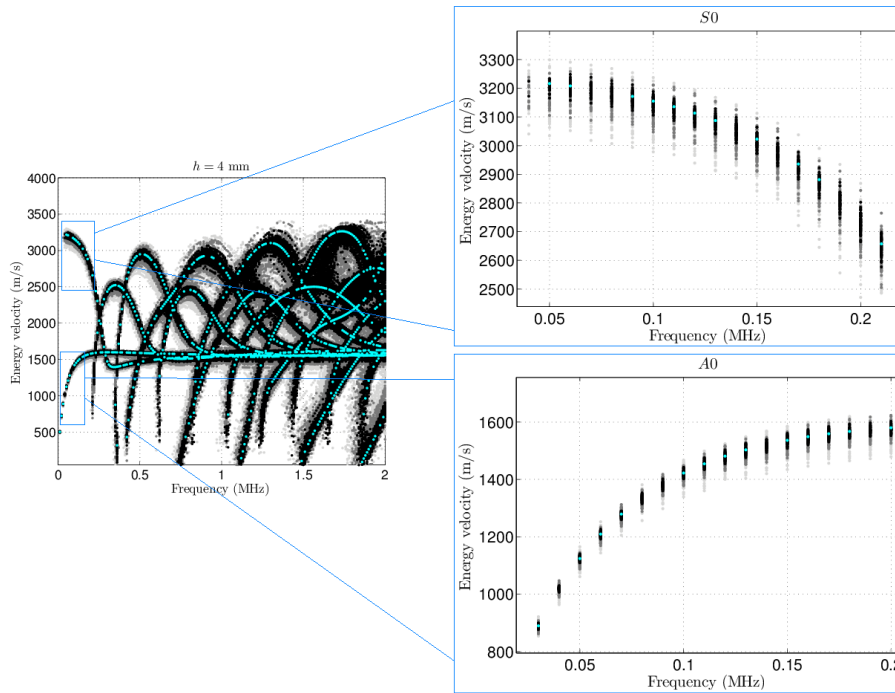


Figure 12: (color online) Energy velocity dispersion curves of thick plate. Deterministic results are plotted in cyan color.

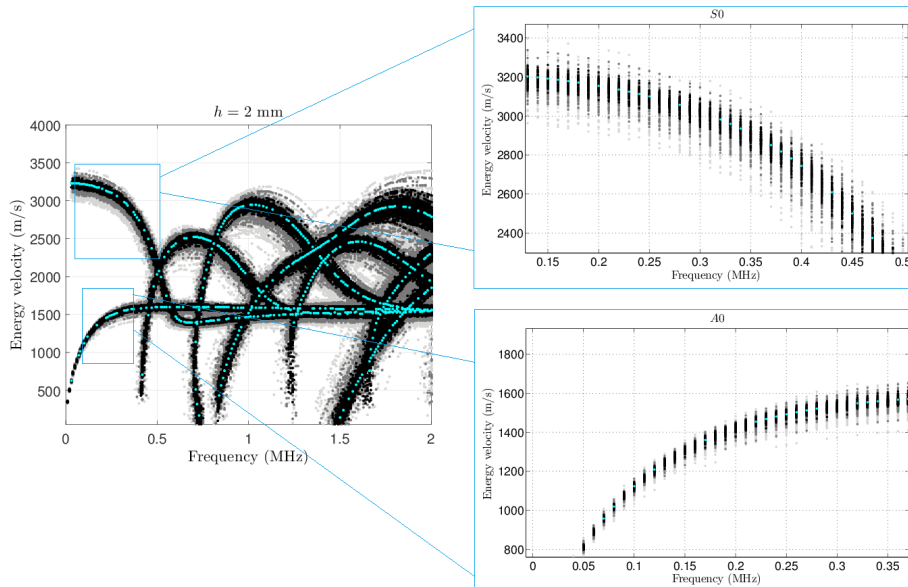


Figure 13: (color online) Energy velocity dispersion curves of thin plate.

ered a two-dimensional model in which the random fluctuation of elastic modulus properties in out-plan direction is neglected. It would be interesting extend the present study into a three-dimensional configuration. In the context of qualitative ultrasound testing of long bones, 3D waveguide models (with idealized circular section or with real geometry cross section) may be employed for investigating the effect the random heterogeneity of elastic moduli is introduced in the section's plan.

It is worth noting that, the numerical procedure proposed in this paper is not only limited for long bone ultrasound characterization but also for other non-destructive evaluation applications in engineering, in which the random heterogeneous material properties should be taken into account,

A. Appendix: Confidence regions *via* the quantile method

A procedure based on the quantile method is performed for estimating the confidence regions of random variables displacement U_1 and U_2 . The confidence region of u_1 is limited by a lower envelope and an upper envelope, denoted by u_1^- and u_1^+ , respectively:

$$\mathbb{P}(u_1^- < U_1 \leq u_1^+) = P_c, \quad (31)$$

where $\mathbb{P}(A)$ denotes the probability measure of an event A .

Let F_{U_1} be the cumulative distribution function of U_1 defined by $F_{U_1}(u_1) = \mathbb{P}(U_1 \leq u_1)$. The p -th quantile ($p \in]0, 1[$) of F_{U_1} is defined by:

$$\zeta(p) = \inf \left\{ r : F_{U_1}(u_1) \geq p \right\}. \quad (32)$$

The lower and upper envelopes u_1^- and u_1^+ are defined by:

$$u_1^- = \zeta \left(\frac{1 - P_c}{2} \right), \quad u_1^+ = \zeta \left(\frac{1 + P_c}{2} \right). \quad (33)$$

Let $\tilde{u}_{1(1)} < \dots < \tilde{u}_{1(n_r)}$ be the order statistics associated with $U_1(\phi_1), \dots, U_1(\phi_{n_r})$, we have the following estimations:

$$u_1^- \simeq \tilde{u}_{1j^-}, \quad j^- = \text{fix}[n_r(1 - P_c)/2], \quad (34)$$

$$u_1^+ \simeq \tilde{u}_{1j^+}, \quad j^+ = \text{fix}[n_r(1 + P_c)/2], \quad (35)$$

in which $\text{fix}[\star]$ denotes the integer part of the real number $[\star]$.

References

- [1] Bal, G., Ryzhik, L., 2001. Time reversal for classical waves in random media. *Comptes Rendus de l'Académie des Sciences - Series I - Mathematics* 333, 1041 – 1046.
- [2] Baron, C., 2011. Propagation of elastic waves in an anisotropic functionally graded hollow cylinder in vacuum. *Ultrasonics* 51, 123 – 130.
- [3] Baron, C., Naili, S., 2008. Elastic wave propagation in a fluid-loaded anisotropic waveguide with laterally varying properties. *C.R. Mécanique* 336, 772–730.
- [4] Bathe, K., 1996. *Finite Element Procedures*. Prentice-hall.
- [5] Ben Souf, M., Bareille, O., Ichchou, M., Bouchoucha, F., Haddar, M., 2013. Waves and energy in random elastic guided media through the stochastic wave finite element method. *Physics Letters A* 377, 2255 – 2264.
- [6] Bouchoucha, F., Ichchou, M., Haddar, M., 2013. Guided wave propagation in uncertain elastic media. *Ultrasonics* 53, 303 – 312.
- [7] Chen, J., Cheng, L., Su, Z., Qin, L., 2013. Modeling elastic waves in coupled media: Estimate of soft tissue influence and application to quantitative ultrasound. *Ultrasonics* 53, 350 – 362.
- [8] Chen, J., Su, Z., 2014. On ultrasound waves guided by bones with coupled soft tissues: A mechanism study and *in vitro* calibration. *Ultrasonics* 54, 1186 – 1196.
- [9] Chimenti, D., Rokhlin, S., 1990. Relationship between leaky lamb modes and reflection coefficient zeroes for a fluid coupled elastic layer. *The Journal of the Acoustical Society of America* 88, 1603–1611.
- [10] Cieszko, M., Drelich, R., Pakula, M., 2016. Wave dispersion in randomly layered materials. *Wave Motion* 64, 52 – 67.
- [11] Cowin, S., 2001. *Bone mechanics handbook*. 2nd ed., CRC Press, Boca Raton, FL.
- [12] Desceliers, C., Soize, C., Grimal, Q., Haiat, G., Naili, S., 2008. A time-domain method to solve transient elastic wave propagation in a multilayer medium with a hybrid spectral-finite element space approximation. *Wave Motion* 45, 383 – 399.
- [13] Desceliers, C., Soize, C., Naili, S., Haiat, G., 2009. Determination of the random anisotropic elasticity layer using transient wave propagation in a fluid-solid multilayer: Model and experiments. *The Journal of the Acoustical Society of America* 125, 2027–2034.
- [14] Desceliers, C., Soize, C., Naili, S., Haiat, G., 2012. Probabilistic model of the human cortical bone with mechanical alterations in ultrasonic range. *Mechanical Systems and Signal Processing* 32, 170 – 177.
- [15] Dong, X., Guo, X., 2004. The dependence of transversely isotropic elasticity of human femoral cortical bone on porosity. *Journal of Biomechanics* 37, 1281–1287.
- [16] Fabro, A., Ferguson, N., Jain, T., Halkyard, R., Mace, B., 2015. Wave propagation in one-dimensional waveguides with slowly varying random spatially correlated variability. *Journal of Sound and Vibration* 343, 20 – 48.
- [17] Ichchou, M., Bouchoucha, F., Ben Souf, M., Dessombz, O., Haddar, M., 2011. Stochastic wave finite element for random periodic media through first-order perturbation. *Computer Methods in Applied Mechanics and Engineering* 200, 2805–2813.
- [18] Jaynes, E., 1957a. Information theory and statistical mechanics. *The Physical Review* 106, 620–630.
- [19] Jaynes, E., 1957b. Information theory and statistical mechanics. II. *The Physical Review* 108, 171–190.
- [20] Kaufman, J.J., Luo, G., Siffert, R., 2008. Ultrasound simulation in bone. *IEEE Transactions on Ultrasonics, Ferroelectrics and Frequency Control* 55, 1205.
- [21] Laugier, P., Haiat, G. (Eds.), 2011. *Bone Quantitative Ultrasound*. Springer.
- [22] Lee, K., Yoon, S., 2016. Propagation of time-reversed lamb waves in acrylic cylindrical tubes as cortical-bone-mimicking phantoms. *Applied Acoustics* 112, 10 – 13.
- [23] Naili, S., Nguyen, V.H., Vu, M.B., Desceliers, C., Soize, C., 2015. Modeling of transient wave propagation in a heterogeneous solid layer coupled with fluid: Application to long bones. *The Journal of the Acoustical Society of America* 137, 668–678.
- [24] Nayfeh, A., Chimenti, D., 1988. Ultrasonic wave reflection from liquid-coupled orthotropic plates with application to fibrous composites. *Journal of Applied Mechanics* 55, 863–870.
- [25] Nayfeh, H., 1995. *Wave Propagation in Layered Anisotropic Media*. Elsevier.
- [26] Nguyen, V.H., Abdoulatuf, A., Desceliers, C., Naili, S., 2016. A probabilistic study of reflection and transmission coefficients of random anisotropic elastic plates. *Wave Motion* 64, 103 – 118.
- [27] Nguyen, V.H., Lemaire, T., Naili, S., 2010. Poroelastic behaviour of cortical bone under harmonic axial loading: A finite element study at the osteonal scale. *Medical Engineering & Physics* 32, 384 – 390.
- [28] Nguyen, V.H., Naili, S., 2012. Simulation of ultrasonic wave propagation in anisotropic poroelastic bone plate using hybrid spectral/finite element method. *International Journal for Numerical Methods in Biomedical Engineering* 28, 861–876.
- [29] Nguyen, V.H., Naili, S., 2013. Ultrasonic wave propagation in viscoelastic cortical bone plate coupled with fluids: a spectral finite element study. *Computer Methods in Biomechanics and Biomedical Engineering* 16, 963–974.
- [30] Nicholson, P., Moilanen, P., Karkkainen, T., Timonen, J., Cheng, S., 2002. Guided ultrasonic waves in long bones: modelling, experiment and *in vivo* application. *Physiological Measurement* 23, 755–768.
- [31] Parra, J., Hackert, C., Ababou, R., Sablik, M., 1999. Dispersion and attenuation of acoustic waves in randomly heterogeneous media. *Journal of Applied Geophysics* 42, 99 – 115.
- [32] Pereira, D., Haiat, G., Fernandes, J., Belanger, P., 2017. Simulation of acoustic guided wave propagation in cortical bone using a semi-analytical finite element method. *The Journal of the Acoustical Society of America* 141, 2538–2547.

- [33] Rose, J., 1999. Ultrasonic waves in solid media. Cambridge University Press.
- [34] Rosi, G., Nguyen, V.H., Naili, S., 2016. Numerical investigations of ultrasound wave propagating in long bones using a poroelastic model. *Mathematics and Mechanics of Solids* 21, 119–133.
- [35] Royer, D., Dieulesaint, E., 2000. Elastic wave in solids I. free and guides propagation. Springer.
- [36] Soize, C., 2001. Maximum entropy approach for modeling random uncertainties in transient elastodynamics. *The Journal of the Acoustical Society of America* 109, 1979–1996.
- [37] Soize, C., 2006. Non-gaussian positive-definite matrix-valued random fields for elliptic stochastic partial differential operators. *Computer Methods in Applied Mechanics and Engineering* 195, 26–64.
- [38] Ta, D.A., Huang, K., Wang, W.Q., Wang, Y.Y., Le, L., 2006. Identification and analysis of multimode guided waves in tibia cortical bone. *Ultrasonics* 44, Supplement, e279 – e284. Proceedings of Ultrasonics International (UI'05) and World Congress on Ultrasonics (WCU).
- [39] Tatarinov, A., Sarvazyan, N., Sarvazyan, A., 2005. Use of multiple acoustic wave modes for assessment of long bones: Model study. *Ultrasonics* 43, 672 – 680.
- [40] Tran, T., L.H., L., Sacchi, M., Nguyen, V., 2018. Sensitivity analysis of ultrasonic guided waves propagating in trilayered bone models: a numerical study. *Biomech Model Mechanobiol* 17, 1269–1279.
- [41] Wang, L., Fritton, S., Cowin, S., Weinbaum, S., 1999. Fluid pressure relaxation depends upon osteonal microstructure: modeling an oscillatory bending experiment. *Journal of Biomechanics* 32, 663–672.
- [42] Xu, K., Liu, D., Ta, D.A., Hu, B., Wang, W., 2014. Quantification of guided mode propagation in fractured long bones. *Ultrasonics* 54, 1210 – 1218.